PROTON STRUCTURE MEASUREMENTS AT HIGH Q^2 AND LARGE X

K. WICHMANN

Institute of Experimental Physics, Hamburg University
Luruper Chaussee 149,
22607 Hamburg, Germany
E-mail: kklimek@mail.desy.de

Proton structure measurements at high Q^2 and x, performed by the H1 and ZEUS Collaborations at the HERA accelerator, are reviewed. Neutral and charge current deep inelastic scattering cross sections and structure function measurements are presented. A new method employed to measure the NC cross section up to Bjorken-x values equal to one is described. The review also discusses the ZEUS-JETS PDF fits which include jet data giving direct access to the gluon densities. An estimate on the impact of HERA II data on the PDFs and their influence on the LHC measurements are mentioned.

1. Introduction

Precise knowledge of proton parton distribution functions (PDFs) is crucial for understanding proton structure. Additionally it is required for any cross-section calculation at hadron colliders for Standard Model (SM) physics as well as for the discovery of physics beyond the SM.

The PDFs are usually determined in global fits within the DGLAP formalism [1−4] at next-to-leading order (NLO) in QCD. These fits use data from many different experiments, with the inclusive cross-section data from deep inelastic scattering (DIS) experiments providing the major source of information. The wide kinematic range covered by the HERA DIS data [5−7], as well as their precision, has allowed the determination of PDFs across a broad range of phase space spanned by the fractional proton momentum, Bjorken-x, carried by the struck quark, and the negative squared four-momentum transfer Q^2. This paper reviews the measurements at high Q^2 and x performed by the H1 and ZEUS Collaborations at the HERA accelerator.

2. Cross Section Measurements and Structure Functions

The differential cross section for lepton-nucleon ($l^{\pm}N$) NC DIS is given in terms of structure functions by

$$\frac{d^2\sigma^{NC}(l^{\pm}N)}{dxdQ^2} = \frac{2\pi\alpha^2}{xQ^4}[Y_+F_2(x,Q^2) \mp Y_-xF_3(x,Q^2) - y^2F_L(x,Q^2)], \quad (1)$$

where α is the electromagnetic fine structure constant, y is the inelasticity parameter and $Y_{\pm} = 1 \pm (1-y)^2$. The longitudinal structure function, F_L , is significant only at large y and low Q^2 and is not discussed in this paper. The structure functions F_2 and xF_3 are directly related to quark distributions and their Q^2 dependence is predicted by perturbative QCD. For Q^2 up to around 1000 GeV^2 the charged lepton-hadron cross section is dominated by photon exchange and the F_2 structure function. For values of x lower than about 10^{-2} F_2 is sea-quark dominated and its Q^2 dependence is driven by the gluon density. That is why HERA can provide crucial information on gluon and quark distributions. The structure function F_3, which provides information on valence quark distributions, is dominated by a parity-violating term and thus makes a significant contribution only at large Q^2. The structure function F_3 is measured by subtracting the NC cross sections of electron-proton and positron-proton DIS. Fig.1 shows xF_3 at fixed values of Q^2 as a function of x. The measurements of the H1 [8] and ZEUS [9] Collaborations are in good agreement. The expectation of the SM, evaluated with the CTEQ6D [16] PDFs, gives a good description of the data. So far the biggest uncertainty comes from the smaller e^-p sample. With already about ten times more e^-p data at HERA II, more significant results are expected soon.

The charged-current (CC) interactions are sensitive to the flavor of the valence distributions at high x because their (LO) cross sections are given by

$$\frac{d^2\sigma^{CC}}{dxdQ^2}(e^+p) = \frac{G_F^2}{2\pi x}\frac{M_W^4}{(Q^2+M_W^2)^2}x[(\bar{u}+\bar{c}) + (1-y^2)(d+s)], \quad (2)$$

$$\frac{d^2\sigma^{CC}}{dxdQ^2}(e^-p) = \frac{G_F^2}{2\pi x}\frac{M_W^4}{(Q^2+M_W^2)^2}x[(u+c) + (1-y^2)(\bar{d}+\bar{s})], \quad (3)$$

where G_F is the Fermi coupling constant and M_W is the mass of the W-boson and the parton distributions u, d, s, c are functions of x and Q^2. The reduced cross sections, $\tilde{\sigma}$, are defined as

$$\tilde{\sigma} = \left[\frac{G_F^2}{2\pi x}\frac{M_W^4}{(Q^2+M_W^2)^2}\right]^{-1}\frac{d^2\sigma^{CC}}{dxdQ^2}.$$

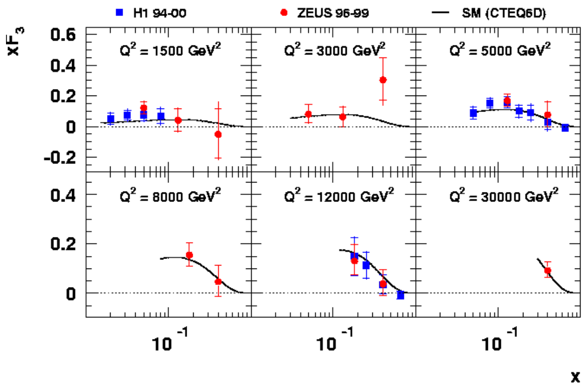

Figure 1. The structure function xF_3 as a function of x for different Q^2 values measured by the H1 (squares) and ZEUS (dots) Collaborations. The inner error bars show the statistical uncertainty, while the outer ones show the statistical and systematic uncertainties added in quadrature. Also shown are SM predictions using CTEQ6D PDFs.

The e^-p CC cross section gives information on the u valence quark at high x. The e^+p CC cross section gives information on the d valence quark at high x, and since the d valence quark distribution is poorly known these data are particularly valuable. Fig.2 shows the e^-p and e^+p reduced cross sections as a function of x, measured by H1 [8,10] and ZEUS [11], compared to SM predictions evaluated using CTEQ6D. The contributions from the PDF combinations $(u+c)$ and $\bar{d}+\bar{s}$ for e^-p and $(d+s)$ and $\bar{u}+\bar{c}$ for e^+p, obtained in the $\overline{\mathrm{MS}}$ scheme from the ZEUS-S fit, are also shown. There is good agreement between the two measurements. The SM prediction evaluated using CTEQ6D gives a good description of the data.

3. High-x Measurement

Due to limitations in beam energies and measurement techniques a direct confrontation with data has not been possible to date for $x \to 1$. The highest measured points in the DIS regime are at $x = 0.75$ [12]. Data at higher x [13,14] exist, but they are in the resonance production region and cannot be easily interpreted in terms of parton distributions. The highest value of x so far for HERA structure function data is $x = 0.65$. A new method [15] was employed to measure the NC cross section up to Bjorken-x values equal to one with the ZEUS detector for $Q^2 > 576$ GeV^2. In most of the DIS events

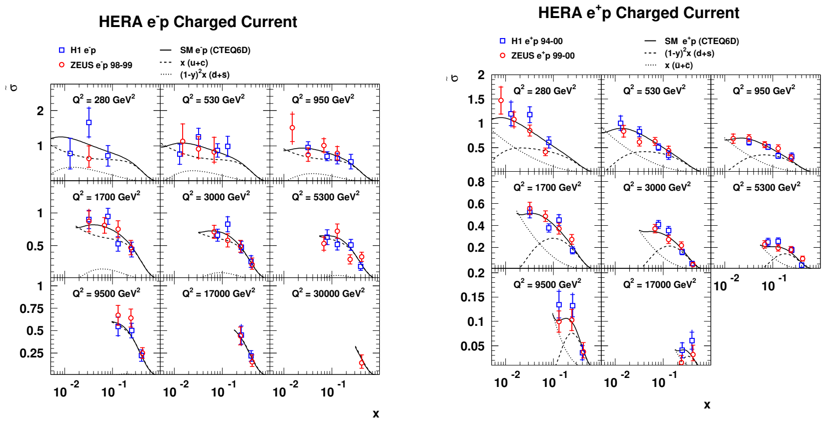

Figure 2. The reduced CC cross section, $\tilde{\sigma}$, as a function of x, for different values of Q^2 for e^-p (left) and e^+p (right) scattering measured by the H1 (squares) and ZEUS (circles) Collaborations. The inner error bars show the statistical uncertainty, while the outer ones show the statistical and systematic uncertainties added in quadrature. The SM expectations calculated using CTEQ6D PDF are shown as full line. The separate contributions from the PDF combinations $x(u+c)$ and $(1-y)^2x(\bar{d}+\bar{s})$ for e^-p, $(1-y)^2x(d+s)$ and $x(\bar{u}+\bar{c})$ for e^+p are indicated by dashed and dotted lines, respectively.

there is a jet present in the detector. As x increases, the jet is boosted in the forward direction and the jet angle decreases. When x is too high, a part of the jet is lost in the beam pipe. The value of x at which this occurs is Q^2 dependent: as Q^2 increases the x value for which jets are well contained increases. In this analysis for $Q^2 > 576$ GeV^2, the electron was scattered at large angles and was well contained in the detector. For the purpose of this analysis the electron and jet information were combined to allow a measurement of the differential cross section up to $x = 1$. Events are sorted into Q^2 and x bins to allow a measurement of the double differential cross section $d^2\sigma/dxdQ^2$. The value Q^2 was calculated using electron information only and the jet energy and angle were used to calculate x for events with a well reconstructed jet. Events with no jet reconstructed within the fiducial volume were assumed to come from high x and were collected in a bin with $x_{\text{Edge}} < x < 1$. These bins were generally large and the form of the PDF is not well known in this region and therefore an integrated cross section was calculated. Events with more than one high energy jet were discarded. The standard selection cuts ensured a background-free and well reconstructed DIS sample for e^+p and e^-p scattering with a good jet with transverse energy greater than 10 GeV. Good agreement between data and

MC simulation is observed for the kinematic, electron and jet variables for the full sample of events. Overall, a small excess of data over MC was observed for zero jet events. Also an offset in the $E - p_Z$ distribution is seen, with the MC distribution slightly lower than the data, but generally the distributions agree well and there is no indication of background in the sample.

The measured Born level cross sections for e^+p are shown in Fig.3 and compared to SM expectations at NLO using the CTEQ6D PDFs. Similar results were obtained for the e^-p data. The double differential cross sections are represented by solid points, and generally agree well with the expectations. The cross section in the highest x bin is the integrated cross section. In this bin, the expected cross section is drawn as a horizontal line, while the measured cross section is displayed by the open symbol.

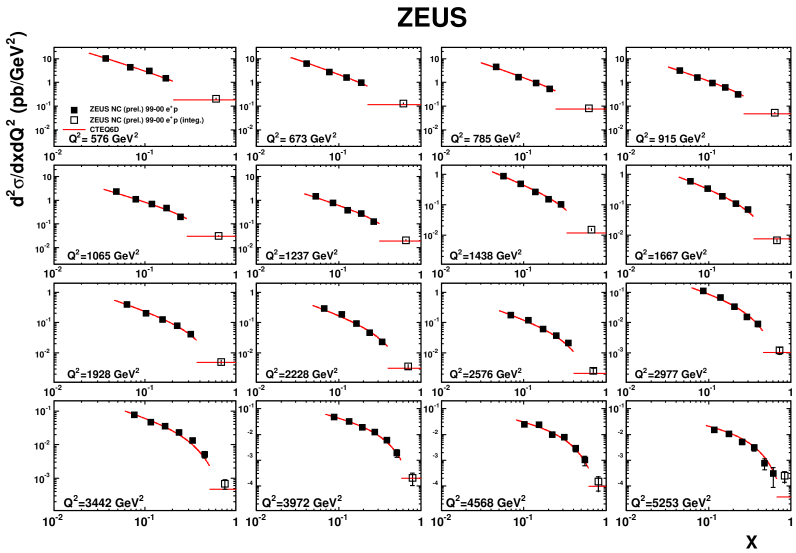

Figure 3. The double differential cross section for e^+p NC scattering (solid squares) and the integral of the double differential cross section divided by the bin width (open squares) compared to the Standard Model expectations evaluated using CTEQ6D PDFs (lines). The inner error bars show the statistical uncertainty, while the outer ones show the statistical and systematic uncertainties added in quadrature.

The measured double differential cross sections generally agree well with the expectations. For the highest x bins, which are in previously unmeasured kinematic ranges, the data has a tendency to lie above the expectations. These data are expected to have an impact on the extraction of the PDFs at the highest values of x, and via sum rules, also on the PDFs at smaller x. Due to the limited statistics the present measurement has a modest impact on the PDFs but the method is developed and HERA II will have significant impact.

4. Jet Data in Global Fits

The gluon density contributes only indirectly to the inclusive DIS cross sections. However it makes a direct contribution to jet cross sections through boson-gluon and quark-gluon scattering. Tevatron high-E_T data [17,18] have been used to constrain the gluon in the fits of MRST [19,20] and CTEQ [16]. However, these data suffer from very large correlated systematic uncertainties from a variety of sources. In the ZEUS-JETS fit [21], ZEUS NC e^+p DIS inclusive jet cross sections [22] and direct photoproduction dijet cross sections [23] have been used to constrain the gluon. The jet cross sections used in this analysis are shown in Fig.4 together with the SM predictions evaluated using the ZEUS-JETS parton densities. The data and predictions agree well.

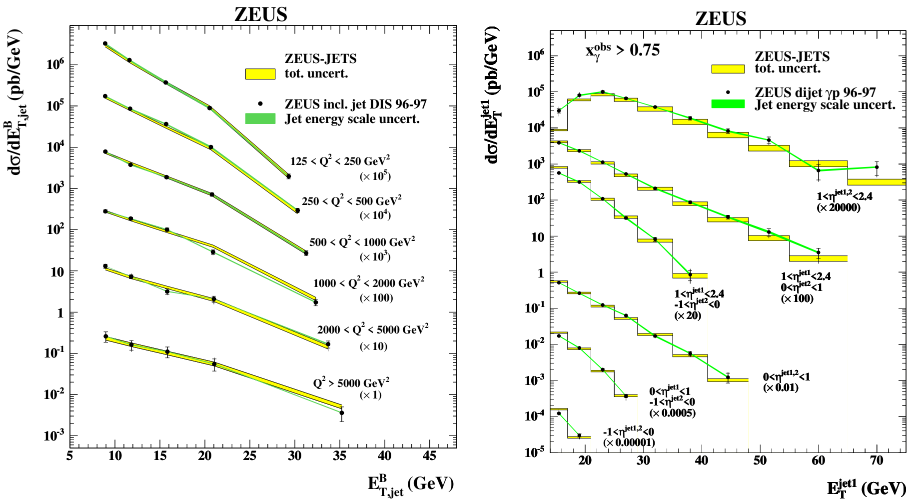

Figure 4. ZEUS-JETS fit compared to ZEUS DIS inclusive jet data (left) and photoproduction dijet data (right), respectively. Each cross section has been multiplied by the scale factor in brackets to aid visibility.

These jet data together with ZEUS data on NC and CC e^+p and e^-p DIS inclusive cross sections [9,11,24–27] were used as inputs to an NLO QCD DGLAP analysis in order to determine the PDFs. The predictions for the jet cross sections are calculated to NLO in QCD and are used in the fit rigorously, rather than approximately as in previous fits [16,19,20]. The details of the fit and the fitting procedure are described in detail elsewhere in these proceedings [28]. The valence, sea and gluon PDFs are compared for the ZEUS-JETS fit and the previous ZEUS-S global PDF analysis in Fig.5. There is good agreement between the ZEUS PDF extractions. In the figure there is also a comparison of the MRST and CTEQ PDFs to the ZEUS-JETS PDFs. Considering the size of the uncertainties on each PDF set, they are compatible with the ZEUS PDFs.

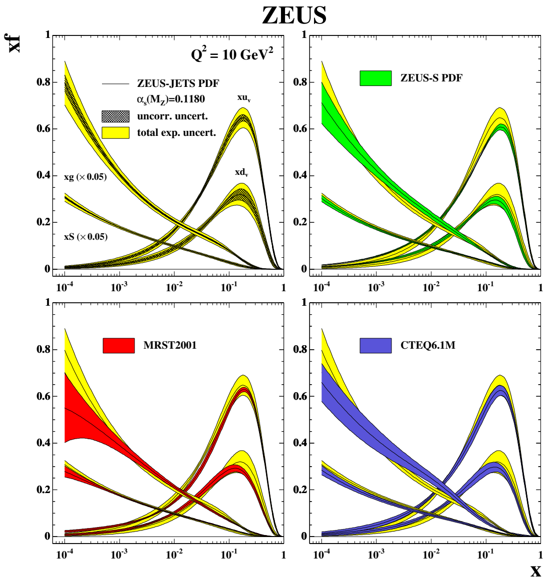

Figure 5. (a) PDFs extracted from the ZEUS-JETS fit. (b) PDFs extracted from the ZEUS-JETS fit compared to ZEUS-S PDFs. (c) PDFs extracted from the ZEUS-JETS fit compared to MRST2001 PDFs. (d) PDFs extracted from the ZEUS-JETS fit compared to CTEQ6.1M PDFs. The total experimental uncertainty bands are shown for each PDF set.

The use of ZEUS data alone eliminates the uncertainty from heavy-target corrections required in global analyses in which the νFe and μD

fixed-target data, together with isospin-symmetry constraints between u and d in the proton and neutron, have been used for determining the valence distributions. It also avoids the difficulties that can sometimes arise from combining data sets from several different experiments, thereby allowing a rigorous statistical treatment of the PDF uncertainties. In the ZEUS-JETS fit the lower Q^2 NC inclusive cross-section data determine the low-x sea and gluon distributions and the high-Q^2 NC and CC inclusive cross sections determine the valence distributions. The jet cross-section data constrain the mid- to high-x gluon density. The gluon and sea distributions are as well determined as the corresponding distributions in the global fits at low x since for all the fits these distributions are determined by the HERA inclusive NC data. The sea distributions at high x are constrained to be similar to those of the ZEUS-S global fit by the choice of the parametrisation. The uncertainties of the gluon have been reduced by the addition of the ZEUS jet data. In Fig.6 the uncertainty of the gluon distribution for fits with and without the jet data are compared.

The shapes of the PDFs are not changed significantly by the addition of jet data. The decrease in the uncertainty on the gluon distribution is significant. In the mid-x range, over the full Q^2 range a decrease in uncertainty by a factor of about two is found.

5. Prospects of HERA Measurements

PDF uncertainties from current global fits are, in general, limited by (irreducible) experimental systematics. In contrast, those from fits to HERA data alone, are largely limited by the statistical precision of existing measurements. Therefore, the impact of future data from HERA is likely to be most significant in fits to HERA data only. HERA II is now running efficiently and is expected to provide a substantial increase in luminosity. This will allow more precise measurements of cross sections that are currently statistically limited, in particular, the high-Q^2 NC and CC data and high-Q^2 and/or high-E_T jet data. In addition to the simple increase in luminosity, recent studies [29] have shown that future jet cross-section measurements, in kinematic regions optimized for sensitivity to PDFs, should have a significant impact on the gluon uncertainties. The effect on the PDF uncertainties, of both the higher precision expected from HERA II and the possibility of optimized jet cross-section measurements, has been estimated in a new QCD fit [29] ("HERA-II projection" fit). For the high-Q^2 inclusive data, a total integrated luminosity of 700 pb^{-1} was assumed, equally di-

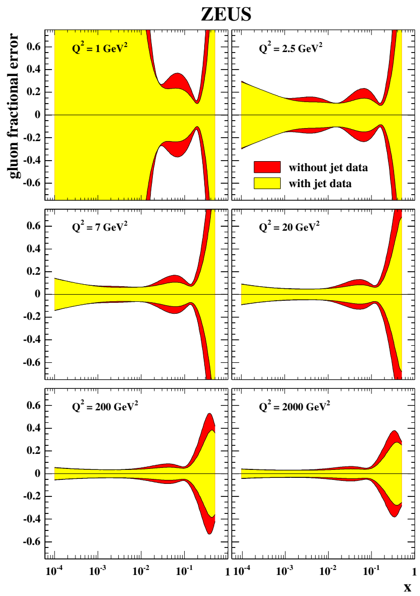

Figure 6. The total experimental uncertainty on the gluon PDF for the ZEUS-JETS fit (central error bands) compared to the total experimental uncertainty on the gluon PDF for a fit not including the jet data (outer error bands). The uncertainties are shown as fractional differences from the central values of the fits, for various values of Q^2. The total experimental uncertainty includes the statistical, uncorrelated and correlated systematic uncertainties and normalization, for both fits.

vided between e^+ and e^- . For the jet data, an integrated luminosity of 500 pb^{-1} was assumed. The central values and systematic uncertainties were taken from the published data in each case. In addition to the assumed increase in precision of the measurements, a set of optimized jet cross sections were also included, for forward dijets in γp collisions, as defined in a recent study [29], assuming luminosity of 500 pb^{-1}. The increased statistical precision of the high-Q^2 data, as assumed in the HERA II projected fit, gives a significant improvement in the valence uncertainties over the whole range of x. For the sea quarks, a significant improvement in the uncertainties at high-x is also observed. In contrast, the low-x uncertainties are not visibly reduced due to the fact that the data constraining the low-x region tends to be at lower-Q^2, which are already systematically limited. This is also the reason why the low-x gluon uncertainties are not significantly reduced. However, the mid-to-high-x gluon, which is constrained by the jet data, is much improved in the HERA II projected fit. About half of the observed reduction in the gluon uncertainties is due to the inclusion of the simulated optimized jet cross sections.

The improvement to the high-x partons, observed in the HERA II projection will be particularly relevant for high-scale physics at the LHC. The prediction using the HERA II projected PDF shows a marked improvement at high jet transverse energy.

References

1. V.N. Gribov and L.N. Lipatov, *Sov. J. Nucl. Phys.* **15**, 438 (1972)
2. L.N. Lipatov, *Sov. J. Nucl. Phys.* **20**, 438 (1975)
3. G. Altarelli and G. Parisi, *Nucl. Phys.* **B20**, 298 (1977)
4. Yu.L. Dokshitzer, *Sov. Phys. JETP* **46**, 641 (1977)
5. ZEUS Collab., S. Chekanov et al., *Phys. Rev.* **D67**, 012007 (2003)
6. H1 Collab., C. Adloff et al., *Eur. Phys. J.* **C21**, 33 (2001)
7. H1 Collab., C. Adloff et al., *Eur. Phys. J.* **C30**, 1 (2003)
8. H1 Collab., C. Adloff et al., *Eur Phys J.* **C30**, 1 (2003)
9. ZEUS Collab., S. Chekanov et al., *Eur. Phys. J* **C28**, 175 (2003)
10. H1 Collab., C. Adloff et al., *Eur Phys J.* **C19**, 269 (2001)
11. ZEUS Collab., S. Chekanov et al., *Eur. Phys. J* **C32**, 16 (2003)
12. BCDMS Collab., A.C. Benvenuti et al., *Phys. Lett.* **B223**, 485 (1989)
13. L.W. Whitlow et al., *Phys. Lett.* **B282**, 475 (1992)
14. M. Osipenko et al., *Phys. Rev.* **D67**, 092001 (2003)
15. ZEUS Collab., S. Chekanov et al., 'Neutral current deep inelastic scattering measurements at high x', paper submitted to LP05 and EPS05 conferences
16. J. Pumplin et al., *JHEP* **0207**, 012 (2001)
17. DØ Collab., B. Abbott et al., *Phys. Rev. Lett.* **82**, 2451 (1999)
18. CDF Collab., T. Affolder et al., *Phys. Rev.* **D64**, 032001 (2001)
19. A.D. Martin et al., *Eur. Phys. J.* **C23**, 73 (2002)
20. A.D. Martin et al., *Eur. Phys. J.* **C28**, 455 (2002)
21. ZEUS Collab., S. Chekanov et al., *Eur. Phys. J.* **C42**, 1 (2005)
22. ZEUS Collab., S. Chekanov et al., *Phys. Lett.* **B547**, 164 (2002)
23. ZEUS Collab., S. Chekanov et al., *Eur. Phys. J.* **C23**, 615 (2002)
24. ZEUS Collab., S. Chekanov et al., *Eur. Phys. J.* **C21**, 443 (2001)
25. ZEUS Collab., S. Chekanov et al., *Eur. Phys. J.* **C12**, 411 (2000)
26. ZEUS Collab., S. Chekanov et al., *Phys. Lett.* **B539**, 197 (2002)
27. ZEUS Collab., S. Chekanov et al., *Phys. Rev.* **D70**, 052001 (2004)
28. A.M. Cooper-Sarkar, these proceedings
29. C. Gwenlan, A. Cooper-Sarkar, C. Targett-Adams, hep-ph/0509220